Inhibitory inputs to avian ITD circuits

Paula T. Kuokkanen[1], Z. Mehnoush Faghani[1], Ira Kraemer[2], Richard Kempter[1,3,4], Catherine E. Carr[2]

Affiliations:

[1] Institute for Theoretical Biology, Humboldt-Universität zu Berlin, 10115 Berlin, Germany

[2] Department of Biology, University of Maryland College Park, College Park, MD 20742

[3] Bernstein Center for Computational Neuroscience Berlin, 10115 Berlin, Germany

[4] Einstein Center for Neurosciences Berlin, 10117 Berlin, Germany

Corresponding author: Catherine Carr, University of Maryland College Park, MD, 20742, USA; cecarr@umd.edu

Keywords: Inhibition, brainstem, avian, auditory

Abstract

In birds, detection of sound source azimuth begins in the nucleus laminaris (NL), which computes interaural time differences (ITDs). Inhibition has been proposed to protect NL neurons from losing ITD sensitivity with increasing sound level, although the nature of this inhibition is incompletely understood. Anatomical studies show GABAergic synapses throughout NL and the first order nuclei, while *in vitro* studies in chicken NL showed that depolarizing, GABAergic IPSPs shorten membrane time constants, perhaps to allow the membrane potential to follow rapid synaptic currents accurately over a range of sound levels. Given the importance of inhibition in regulating auditory brainstem activity, we examined the nature of the inhibitory input to NL *in vivo*.

The Superior Olivary Nucleus (SON) is the major source of descending GABAergic inhibition to the ipsilateral nucleus magnocellularis (NM), nucleus angularis (NA) and NL, and receives excitatory input from NA and NL. We used viral tracers to reveal projections from SON to NL, and characterized response types within SON. In NL, we isolated inhibitory synaptic currents from extracellular field potentials through the iontophoretic application of blockers of GABA (gabazine) or glycine (strychnine). These blockers increase the onset and offset responses evoked by tonal stimuli, but did not shift best ITD. The co-application of gabazine and strychnine revealed supra-linear summation of GABA and glycine. Profiles of synaptic activation revealed more prominent inhibition following stimulus offset, suggesting inputs to NL originate from both the sustained and offset response types of the SON. These heterogeneous responses may represent separate SON neuronal populations.

Introduction

In birds, detection of sound source azimuth begins with the nucleus laminaris (NL), which computes interaural time differences (ITDs). Inhibition has been proposed to protect NL neurons from losing ITD sensitivity when sound levels increase (Grün et al., 1991; Peña et al., 1996; Brückner and Hyson, 1998; Dasika et al., 2005; Nishino et al., 2008; Burger et al., 2011). This inhibition is assumed to be primarily GABAergic, and to originate from the Superior Olivary Nucleus (SON) (Burger et al., 2011). In both barn owl and chicken, the SON receives excitatory input from NA and NL, and projects to the ipsilateral NM, NL and NA (Burger et al., 2005;

Carr et al., 1989; Yang et al., 1999) (Fig. 1). SON has two other major projections; a reciprocal connections to the contralateral SON, and ascending projections to higher-order targets (Conlee and Parks, 1986; Burger et al., 2005). In chickens, these distinct projections are aligned with three fiber tracts, with each tract originating from specific response types (Baldassano and MacLeod, 2024). Thus, these pathways likely originate from different *in vivo* response types in the SON, although it remains to be determined which response types project to which nuclei (Coleman et al., 2011; Tabor et al., 2012; Baldassano and MacLeod, 2024; Nishino et al., 2008; Burger et al., 2011).

SON projections subserve distinct functions in NM, NA, and NL. *In vitro*, in chicken NM, activation of SON inputs regulates firing rate, improves phase selectivity; and sharpens frequency tuning (Fukui et al., 2010). These changes are caused by long-lasting, depolarizing IPSPs in NM that are blockable by bicuculline, a $GABA_A$ receptor antagonist (Monsivais et al., 2000). In NA, inhibition is both GABAergic and glycinergic (Kuo et al., 2009), and contributes to the intensity coding pathway (MacLeod, 2011). In NL, SON-evoked IPSPs are similarly depolarizing and act to increase low threshold K^+ conductances and decrease membrane input resistance (Hyson et al., 1995; Funabiki et al., 1998; Brückner and Hyson, 1998). This inhibition reduces the strength of inputs to the NL with increasing stimulus levels (Kuba et al., 2002; Cook et al., 2003; Tang et al., 2009), in part because expression of the low threshold K^+ conductance reduces the temporal window for summation, effectively increasing the threshold for coincidence of inputs (Hyson et al., 1995; Burger et al., 2011; Tang and Lu, 2012). Thus, inhibition in NL acts to maintain ITD sensitivity by increasing peak-trough contrast. Support for the SON being one source for this inhibition comes from studies of SON lesions in chicken that diminish the contrast between favorable and unfavorable ITDs (Nishino et al., 2008).

Computational models have constrained hypotheses about the role of the SON in ITD tuning. They propose that SON inhibition should be tonic, broadly tuned, and level dependent, and should regulate activity in NM and regulate thresholds in NL (Grün et al., 1991; Peña et al., 1996; Brückner and Hyson, 1998; Dasika et al., 2005; Nishino et al., 2008). In NM, SON inhibition should balance the strength of the inputs from each ear to NM to provide balanced excitation to NL (Burger et al., 2011; Peña et al., 1996; Fukui et al., 2010), which is achieved by mutual

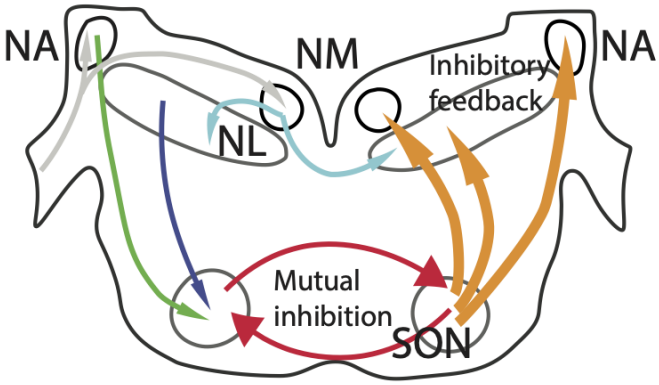

Figure 1: Connections of Auditory Brainstem Nuclei. The Auditory Nerve projects (grey arrows) to Nucleus Angularis (NA) and Nucleus Magnocellularis (NM). NM projects bilaterally to NL (cyan), and both NA and NL project to the SON (blue and green). The SON provides descending inhibition to the auditory brainstem nuclei (orange) as well as mutual inhibition (red).

inhibition between SONs (Fig. 1). Thus, a weak, i.e., quiet, input from the ipsilateral ear should reduce excitation the ipsilateral SON, which reduces inhibition in inhibitory neurons in the contralateral SON, leading to increased contralateral inhibition (Burger et al., 2011; Fukui et al., 2010). Similarly, strong, i.e., loud, input to the ipsilateral ear should inhibit contralateral inhibitory SON neurons and decrease inhibitory drive to contralateral NM (Burger et al., 2011; Fukui et al., 2010; Nishino and Ohmori, 2009). In addition to generating balanced inputs to NL, SON input within NL should regulate thresholds. ITD selectivity in NL is stable over a range of sound levels in both chickens and barn owls (Peña et al., 1996; Burger et al., 2011; Fukui et al., 2010; Nishino and Ohmori, 2009), with the interrelated mechanisms described above underlying this stability (Kuba et al., 2002; Cook et al., 2003; Agmon-Snir et al., 1998; Reyes et al., 1996; Kuba et al., 2005; Hyson et al., 1995).

Given the importance of inhibition in the regulation of activity in NM and NL (Monsivais and Rubel, 2001; Burger et al., 2011, 2015; Burger and Rubel, 2008; Peña et al., 1996), and especially in understanding the effect of hearing loss on the ITD circuit (Burger et al., 2015; Lu et al., 2018), we have examined the nature of the inhibitory input in NL *in vivo* in the barn owl. We used viral tracers to reveal projections from SON to NL, and characterized response types within SON, in combination with the iontophoretic application of blockers of GABA or glycine to isolate inhibitory synaptic currents from extracellular field potentials in NL McColgan et al. (2019).

Methods

Experiments were conducted at the Department of Biology of the University Maryland. Fourteen barn owls (*Tyto alba pratincola*) were used to collect the data presented in this and other studies (McColgan et al., 2019; Kraemer and Carr, 2017). Experimental procedures conformed to NIH Guidelines for Animal Research and were approved by the Animal Care and Use Committee of the University of Maryland. Anaesthesia was induced by intramuscular injections of $10-20$ mg/kg ketamine hydrochloride and $3-4$ mg/kg xylazine. Supplementary doses were administered to maintain a suitable plane of anaesthesia. Body temperature was maintained at 39°C by a feedback-controlled heating blanket.

Recordings were made in a sound-attenuating chamber (IAC, New York). Amplified electrode signals were passed to a threshold discriminator (SD1 (Tucker-Davis Technologies (TDT) Gainesville, FL)) and an analogue-to-digital converter (DD1 (TDT)) connected to a personal computer via an optical interface (OI (TDT)). Acoustic stimuli were digitally generated by custom-made software ('Xdphys' written in Dr. Konishi's lab at Caltech) driving a signal-processing board (DSP2 (TDT)). Acoustic signals were fed to miniature earphones and inserted into the owl's left and right ear canals, respectively.

Anatomical Studies of SON

At a given recording site in NL, we measured frequency tuning and tuning to ITD followed by microinjection of $50-100$ nL virus-containing rAAV2-retro tdTomato solution (Tervo et al., 2016). After a survival time of 2-3 weeks, owls were perfused with 4% paraformaldehyde, and brains blocked and sectioned. Sections were examined using confocal microscopy and reconstructed with the aid of a Neurolucida system.

For immunohistochemical studies of GABAergic terminals, owls were perfused as above, and sectioned at 30 µm. The antiserum against Vesicular Glutamate Transporter (VGAT) was obtained from Antibodies Inc (Davis, CA). Free-floating sections were incubated for 48 h at 4°C in primary antiserum diluted to 1:1000 in PBS containing 0.5% Triton X, followed by 24 h at 4°C in biotinylated secondary antiserum. Sections were subsequently treated according to the avidin-

biotin method (Vector laboratories, Newark, CA). Additional immunohistochemical material included material incubated with antisera against Glutamic Acid Decarboxylase (GAD) (Carr et al., 1989) and material kindly provided by Winer and LaRue, which used rabbit-anti-glycine antiserum (courtesy of R.J. Wenthold; Gly II, 1:1,500), or rabbit-anti-GABA antiserum (from R.J. Wenthold; 1:2,000) (Winer et al., 1995).

Pharmacology

We used iontophoresis to deliver drugs to NL (McColgan et al., 2019). All data were obtained using glass multibarrel electrodes (Carbostar-3 or -4 LT, Kation Scientific, Minneapolis, MN). Microelectrode barrels were filled with gabazine (20 μM SR95531), a $GABA_A$ receptor antagonist and/or strychnine, a glycine receptor antagonist (Sigma, St. Louis, MO). An additional control experiment used saline alone. After control data were collected in the beginning of each experiment, drugs were ejected for $15 - 20$ min, followed by a 20 min washout period, then the cycle repeated. Analyses revealed that repeated washouts did not always return to baseline, especially with strychnine. Thus, we used only the initial condition as control. These are terminal experiments that use urethane as an anesthetic.

In vivo physiology in SON

For these experiments, we recorded in SON with tungsten electrodes ($5 - 20$ MΩ). A grounded silver chloride pellet served as a reference. We measured monaural and binaural frequency tuning, tuning to ITD, and responses to changes in level. Lesions were used to confirm the location of recordings. We used WaveClus MATLAB package for the spike sorting of the waveforms (Quian Quiroga et al., 2004).

Data collection and analysis of synaptic extracellular field potentials in NL

In each recording location, we measured monaural and binaural frequency tuning in the control condition (best frequencies (BF) of the neurophonic ranging 3.2 to 6.8 kHz). For each drug condition (including control conditions), we measured responses to binaural 100-500 ms duration

tone-pips at BF typically at 40 dB SPL, as well as 1-2 additional frequencies around BF, the respective ITD tuning curves (minimum: favourable and unfavourable ITDs) and one or more stimulus amplitudes.

Data recorded during iontophoresis were analyzed using a custom library (pyXdPhys, https://github.com/phreeza/pyXdPhys) by McColgan et al. (2019). Response traces from each drug condition were averaged and filtered (low-pass: <1 kHz, high-pass: >1.5 kHz). The amplitudes of the low pass filtered onsets (offsets) were calculated from the $0 - 50$ ms time span after the stimulus onset (offset) and normalized by the respective control condition onset (offset). We note that over the course of hours, overlapping but not coinciding with the administration of drugs and/or saline, there were small (typically some tens of microseconds) inconsistent phase shifts in the field potential at the stimulus frequency (neurophonic). The phase shifts were not systematically correlated with either the low-pass or the high-pass response amplitudes across the owls (Pearson correlation coefficients for LP: mean $\pm$ SD $= 0.0 \pm 0.4$, ranging from -0.47 to 0.52; for HP 0.0 ± 0.4, ranging from -0.71 to 0.62, with similar variability in all drug groups). These occasional phase shifts may be associated with spatial drift of the brain tissue over hours.

Data availability statement: Data and scripts for reproducing figures 6-9 are available upon request from the authors.

Results

To examine the nature of the inhibitory input to NL from SON we used viral tracers to reveal the projections between NL and SON, and characterized neuronal responses in the SON. We then used iontophoretic application of GABA and glycine blockers *in vivo* into NL, to isolate inhibitory synaptic currents in NL.

SON contains neurons immunopositive for GABA and glycine

The SON is a round nucleus in the rostral pons, ventral to NL (Fig. 1). It contains multiple cell types, some of which are densely labeled by antisera directed against GABA or GAD (Carr et al., 1989; Code et al., 1989; Lachica et al., 1994; Von Bartheld et al., 1989). Barn owl SON

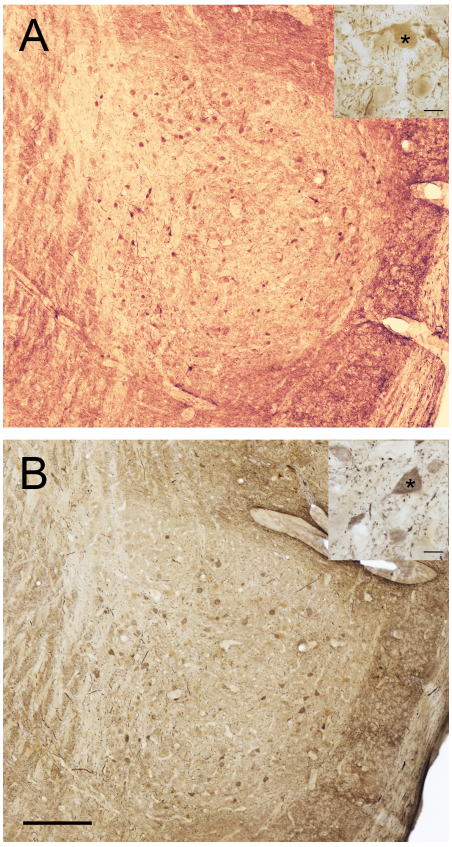

Figure 2: Immunoreactivity in SON. A. Anti-GABA immunoreactive neurons in a transverse section through SON. Inset: immunoreactive neuron (*) surrounded by immunoreactive terminals and unlabeled cell bodies. Bar=20 μm. B: Anti-Glycine immunoreactive neurons in SON. Inset: immunoreactive neuron (*) surrounded by immunoreactive terminals and unlabeled cell bodies. Bar=20 μm. Scale bars for A and B = 200 μm.

contains two sizes of GAD+ neurons: large multipolar cells (cell body area of about (mean $\pm$ SE): 440 ± 30 μm^2, $N = 15$) and medium-sized fusiform cells (cell body area of about 160 ± 20 μm^2, $N = 16$) (Fig. 2A); and there is a third group of large unstained neurons (Carr et al., 1989). The SON also contains a similar population of neurons labeled by antisera against glycine in chicken (Coleman et al., 2011) and in barn owl (Fig. 2B). There are two sizes of glycine+ neurons: large multipolar cells (cell body area of about 440 ± 40 μm^2, $N = 12$) and medium-sized fusiform cells (cell body area of about 218 ± 8 μm^2, $N = 18$) (Fig. 2B). The sizes of the neurons in each size group were not significantly different between the GAD+ and glycine+ populations when corrected for multiple comparisons (Student's 2-population tests, Šidák-correction for $p = 0.05$, Abdi, 2007). Without double label immunohistochemical studies, we were unable to determine

whether SON neurons co-expressed GABA and glycine. Nevertheless, labeled neurons fell into similar size classes (see above), and immunohistochemical evidence has suggested that GABA and glycine may be co-released at SON targets, and glycinergic responses have been shown in NA, NL, and SON (Kuo et al., 2009; Fischl et al., 2014; Coleman et al., 2011; Fischl and Burger, 2014).

Connections of SON

It is likely that at least some of the GABAergic and glycinergic immunolabeled neurons in SON project to NA, NL, and NM, and form perisomatic terminals in NL and NM (see Fig. 5) (Code et al., 1989; Lachica et al., 1994; Coleman et al., 2011; Nishino et al., 2008; Fukui et al., 2010). We note, however, that the two SON are reciprocally connected, and Burger et al. (2011) have proposed that this contralateral projecting pathway is also inhibitory. Thus, we cannot assume that all inhibitory neurons project back to NA, NL, and NM.

To identify which SON neurons projected to NL, we injected rAAV2 into NL (Fig. 3). Injections in 3 barn owls confirmed that SON projects ipsilaterally to NL in the barn owl (Takahashi and Konishi, 1988). In SON, both large (mean ± SE: 430 ± 30 μm^2, $N = 11$) and medium sized (210 ± 20 μm^2, $N = 9$) neurons were retrogradely labeled after these injections (Fig. 3A). The neuron sizes of both the medium-sized and the large-sized population were not significantly different in size from either the relative GAD+ populations or glycine+ populations described in the previous section (all $p > 0.2$, Student's 2-population tests.) In addition, Fig. 3B shows labeled neurons, and NL axons both passing through and terminating in SON. The additional presence of a small number of labeled contralateral SON neurons (not shown) indicates that barn owl NL receives a weaker projection from the contralateral SON.

In vivo physiology in SON

The SON is morphologically heterogeneous and projects to multiple targets (Figs. 1–3) (Takahashi and Konishi, 1988; Baldassano and MacLeod, 2024). Given the heterogeneity of the SON cell types and the array of response types found in chicken (Tabor et al., 2012; Lachica et al., 1994), barn owl SON seemed likely to contain multiple response types. We therefore characterized

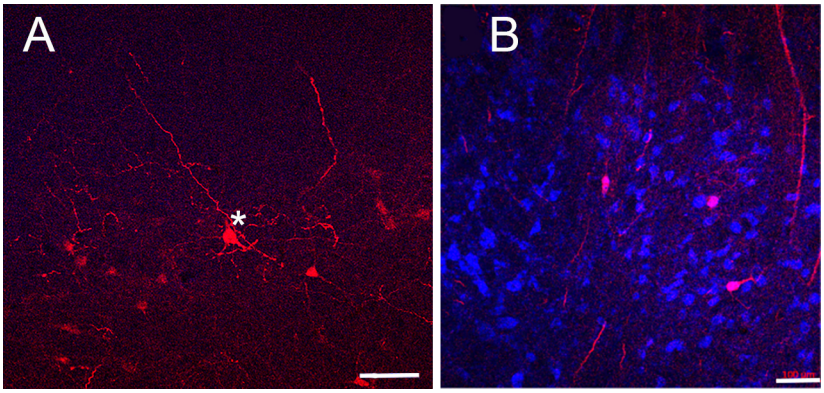

Figure 3: SON Projection Neurons. A. Injection of rAAV2-retro tdTomato into NL yielded two morphological types of projection neuron in SON, of large (*) and medium size. B. rAAV2-retro labeled SON neurons with labeled NL axons. Blue neurotrace counterstain. Scale bar=100 μm

barn owl SON responses *in vivo* in 7 owls. Lesions were used to confirm the recording locations (Fig. 4D). We isolated 70 single units that responded to auditory stimuli. Most units (65 out of 70) recorded responded preferentially to binaural noise and showed broad frequency tuning with low firing rates.

The SON included several response types: sustained, primary-like, off, onset, and on-off. Sustained responses, including primary-like responses (Fig. 4AB), were the most common (70%, $n = 50$), followed by 13% off responses (Fig. 4C) and altogether 17% onset and on-off responses (not shown). There was potential for separating sustained response types into primary-like and sustained (Fig. 4A, B), but these two response types were grouped because their firing rates revealed a continuous distribution. Off-response units fired vigorously after the stimulus ended (Fig. 4C). Based on the shape of the rate-level function of binaural noise stimuli from $15 - 70$ dB SPL, most units demonstrated monotonic rate level curves, and most were excited by both ears. Only about 21% of the 70 SON recordings were ITD sensitive, with ITD sensitivity distributed among all response types.

GABAergic and Glycinergic terminals in NL

The projection from the SON to NL is marked by an oblique lateral to medial axon tract that descends from SON to NL, composed of fine axons that project into NL. Each NL neuron is surrounded by a network of terminals, which can be labeled by antibodies against VGAT. VGAT

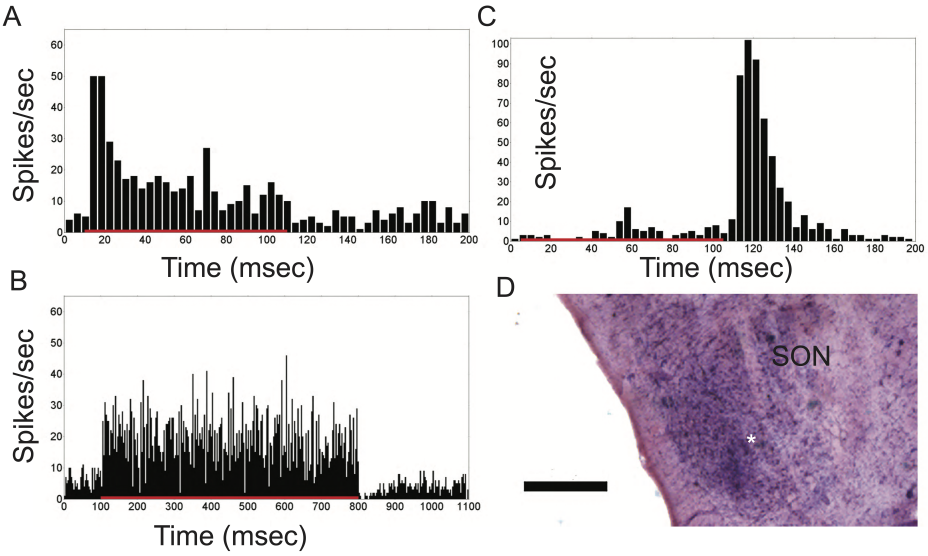

Figure 4: SON Response Types. A. Peristimulus time histogram (PSTH) of a cell with a primary-like response, with an initial peak followed by tonic firing throughout the duration of the stimulus ($10-110$ ms, red bar). B. PSTH of a cell with a sustained response, which typically fires throughout the stimulus. C. PSTH of an offset response cell, which has a high response following the stimulus. D. Following several experiments, recording sites were confirmed by the presence of a lesion from the recording electrode (*). Scale bar=500 µm.

labels both glycinergic and GABAergic terminals (MacLeod and Pandya, 2022) (Fig. 5).

GABAergic terminals may also be labeled with antisera against GAD. Comparisons of GAD and VGAT material revealed similar numbers of terminals per cell. Each NL neuron is surrounded by about 53 ± 14 (mean $\pm$ SD, $n = 80$) GAD+ and 58 ± 17 ($n = 96$) VGAT+ terminals, with the exception of the low best frequency (less than 1 kHz) region which has a higher terminal density (Carr et al., 1989; Nishino et al., 2008).

Pharmacology in NL

To examine the role of the GABAergic innervation in NL, we isolated inhibitory synaptic currents from the extracellular field potential through the iontophoretic application of blockers of $GABA_A$ receptors. Inhibition in ITD coding has been the subject of numerous studies (for reviews, see Roberts et al., 2013; Yin et al., 2019). It has, however, been difficult to examine the effects of GABA on ITD sensitivity *in vivo* in NL (Takahashi and Konishi, 2002). We therefore developed an approach to isolate GABAergic responses based on our previous analysis of AMPA sensitive

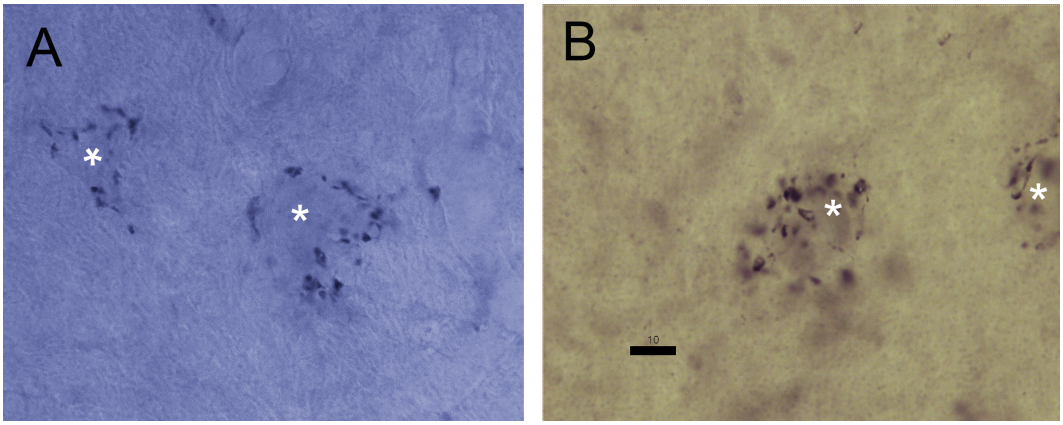

Figure 5: GABAergic Terminals in NL. A. NL neurons (*) surrounded by perisomatic VGAT+ terminals. Note that NL neurons have very short dendrites. B. NL neurons (*) surrounded by perisomatic GAD+ terminals. Scale bar for both=10 µm.

responses in NL (McColgan et al., 2019). In that study, we isolated *in vivo* AMPA sensitive synaptic responses from the neurophonic in NL (McColgan et al., 2019), using iontophoretic application of the antagonist NBQX to reveal synaptic contributions to the extracellular field potential (EFP) (Kuba et al., 2002; Cook et al., 2003).

In a similar approach, we used gabazine to block synaptic currents in NL, since *in vitro* studies in chick had shown both presynaptic GABA release and postsynaptic receptor subtypes in NL (Tang and Lu, 2012), with activity-dependent responses to sensory manipulations (Lu et al., 2018; Fischl and Burger, 2014; Fischl et al., 2014). We compared control and gabazine responses (Fig. 6A,C) during tone-burst stimuli averaged over all trials in the control condition (blue) and during gabazine application (orange, overlap brown). In low pass filtered responses, we subtracted gabazine responses from control conditions to reveal synaptic contributions to the EFP. We found that upon iontophoresis of gabazine, low pass filtered responses (Fig. 6A,B) increased in amplitude, consistent with blockage of inhibition. Our results are consistent with *in vitro* studies in chick (Burger et al., 2011) and *in vivo* and theoretical studies in owl (Peña et al., 1996). Synaptic potentials varied between experiments, presumably because of differences in electrode position (McColgan et al., 2019).

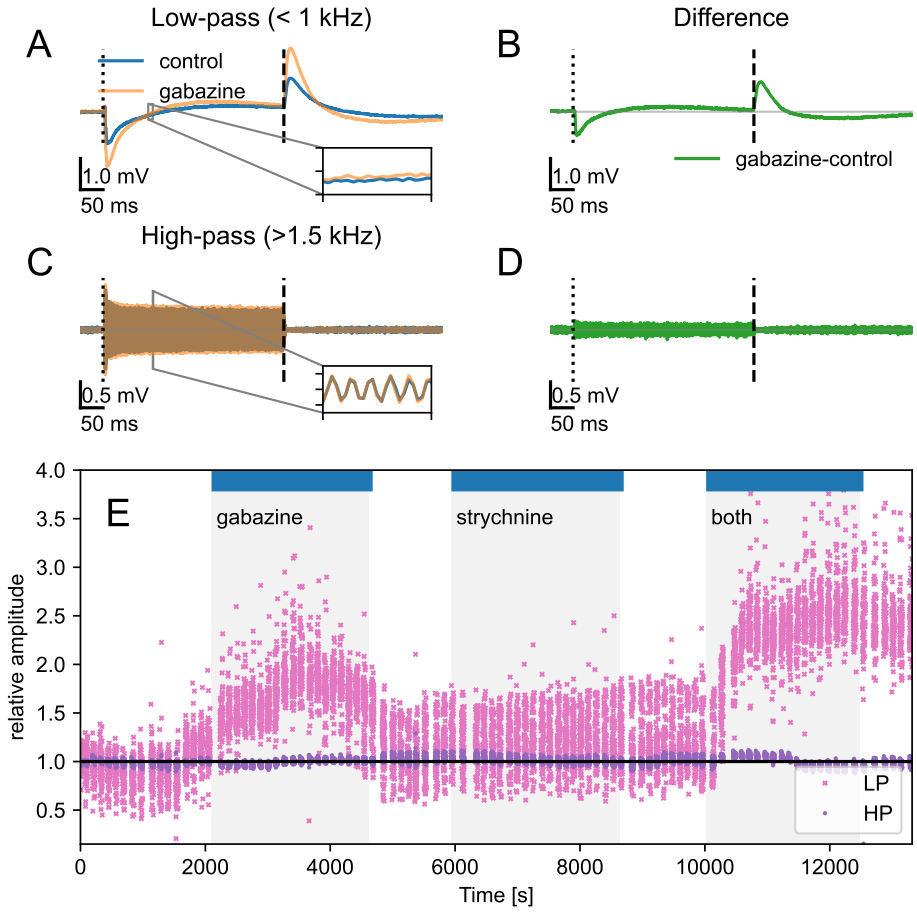

Figure 6: Separability of Synaptic Potentials. Gabazine iontophoresis alters extracellular field potentials in NL, with averaged low-pass filtered responses in control (blue) and during gabazine application (orange; overlap in brown). Stimulus frequency 5600 Hz, amplitude 40 dB, ITD: 30 μs. Stimulus onset (50 ms): dashed lines in A-D, stimulus offset (450 ms): dash-dotted lines in A-D. **A.** Low-pass ($<$ 1 kHz) filtered EFP responses. Inset: a 10-ms (0.5-mV) excerpt for detail. **B.** Difference between the low-pass filtered responses in drug and control conditions reveals synaptic potentials.
C. High-pass ($>$ 1.5 kHz) filtered EFP responses. There is no change in the envelope amplitude, but a phase shift -9 μs of the neurophonic. Inset: a 1-ms (1.5-mV) excerpt for detail.
D. Difference between the high-pass filtered responses in drug and control conditions shows that the phase shift remains constant. **E.** The response amplitude of the high-pass (HP) filtered sustained response (standard deviation of the neurophonic 50-400 ms after stimulus onset) and of the low-pass (LP) filtered onsets (average of the trace 0-50 ms after stimulus onset). All stimulus conditions during the experiment are shown (amplitudes: 30 and 40 dB SLP, stimulus frequencies: 5.3 and 5.6 kHz, ITDs: -30 and 60μs, resulting in 8 different stimulus combinations), each normalized with the average respective response in the initial control condition with no iontophoresis (0-2100 sec).

In vitro data support co-release of GABA and glycine from SON targets, with physiological responses to glycine shown in NA, NM, NL and SON (Kuo et al., 2009; Coleman et al., 2011; Fischl et al., 2014). We isolated glycine-sensitive synaptic responses from the neurophonic in NL *in vivo* using iontophoretic application of the antagonist strychnine. Similar to the gabazine condition, we compared strychnine responses with the control condition (Fig. 6E). In the example shown, strychnine iontophoresis was associated with an increase in the amplitude of the low-pass filtered responses at both onset and offset amplitude, for all of the stimulus conditions. There was no significant change in the amplitude of the high-pass filtered response.

Drug-insensitivity of neurophonic ITD tuning.

The ITD tuning of the high-frequency EFP ('neurophonic') was not affected by either drug (Fig. 7). The neurophonic is composed almost exclusively of the incoming axonal spikes (Kuokkanen et al., 2010, 2013), and was not expected to change with modified inhibitory synaptic currents.

There were sometimes small (typically tens of microseconds) drifts in the neurophonic phase during the hours of recording time, related to the exact location of the electrode with respect to the tissue i.e., the delay line axons. These drifts typically did not coincide with the time of the drug injections, and explained small shifts in the ITD tuning (e.g. Fig. 7A).

The synaptic components of the field potential, i.e. the onset and offset, as revealed by the drugs, were not ITD tuned (Fig. 7B,C). This finding was consistent with our SON recordings, where only about 21% of the SON neurons were ITD tuned. Furthermore, the SON projections into NL appear widespread (Nishino et al., 2008), which is also inconsistent with the precise mapping of ITD. It remains to be tested whether the ITD tuning of postsynaptic NL neurons could be be modified by inhibition: showing postsynaptic ITD modulation in the EFP remains challenging (Kuokkanen et al., 2013, 2018) and was not possible in our data set. It is likely that postsynaptic ITD tuning is also unaffected by inhibition, since a prior study that combined iontophoresis of GABA or muscimol (a $GABA_A$ receptor agonist) in NL with recordings in the optic tectum, did not show changes in best ITD (Takahashi and Konishi, 2002).

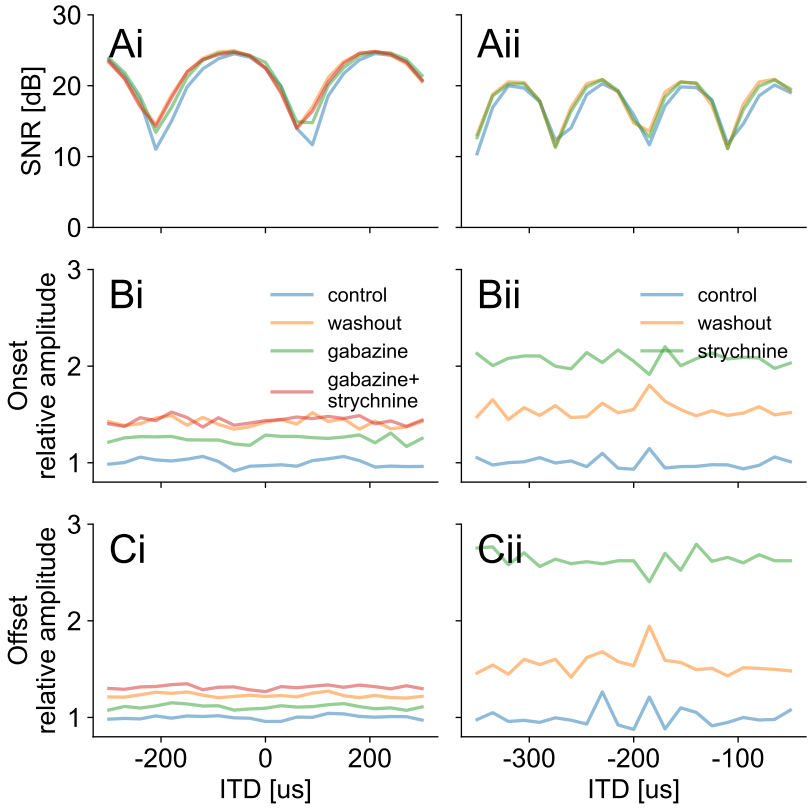

Figure 7: ITD Tuning of the Neurophonic was not Altered by Gabazine or Strychnine. Representative examples of recordings with gabazine and strychnine from two different birds (Ai and Aii). **A.** The signal-to-noise ratio of the neurophonic, i.e. spectral peak at the stimulus frequency wrt. background spectrum (Kuokkanen et al., 2010), showed strong ITD tuning that was not systematically modulated by the application of synaptic blockers. **B,C.** The low-pass filtered onset (B) and offset (C) were increased both by gabazine (i) and by strychnine (ii) application but not ITD-modulated. The values in B,C are normalized by the average of the respective control condition across all ITDs.

Differential Effects of Gabazine and Strychnine.

Since GABA and glycine have been shown to be co-released from SON targets in vitro (Kuo et al., 2009; Coleman et al., 2011; Fischl et al., 2014), we also studied interactions of the two drugs (Fig. 8). Simultaneous injection of gabazine and strychnine revealed a larger synaptic component than the sum of independent injections (Fig. 8Diii, pink line). The interaction component was larger, with a longer duration at the tone offset in comparison to the onset.

For the population data, we took advantage of the ITD insensitivity of the onset and offset responses, averaging the responses across all ITDs for more robust results. For iontophoresis

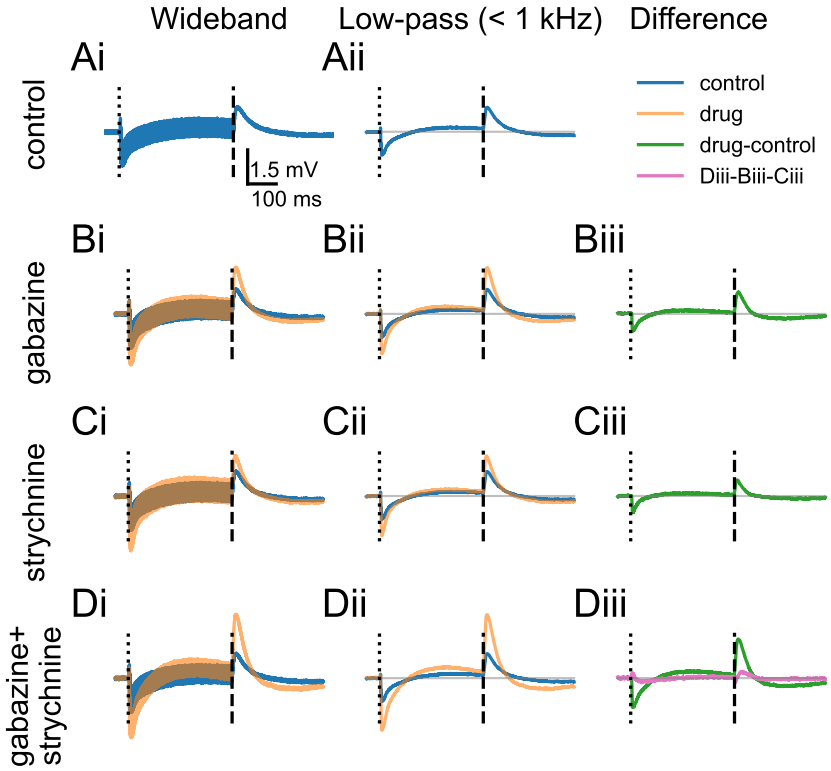

Figure 8: Different Effects of Gabazine and Strychnine. Bird and stimulus: same as in figure 6. **A.** Control condition: i) wide-band response, ii) low-pass filtered response (< 1 kHz). **B.** Gabazine, i-ii) control (blue) and drug condition (orange) shown; overlap in brown; iii) difference to control condition. **C.** Strychnine. **D.** Gabazine+strychnine applied simultaneously. Diii) Pink: the difference of the synaptic currents when both drugs applied simultaneously (green line in Diii) and the sum of separately applied drugs (Biii and Ciii) reveals the supra-linear effect of GABA and glycine.

of either drug, the effect of the strychnine in the population were larger than that of gabazine. Both drugs had a larger effect at tone offset than at tone onset (Fig. 9AB), and simultaneous drug application had a larger effect than expected from the sum of independent drug applications (Fig. 9Civ).

The amplitude of the onset and offset responses increased with level (not shown) (Peña et al., 1996; Köppl and Carr, 2003), while the ratio of the drug/control stayed roughly level-independent (Fig. 9C) in the birds in which we recorded a broad amplitude range.

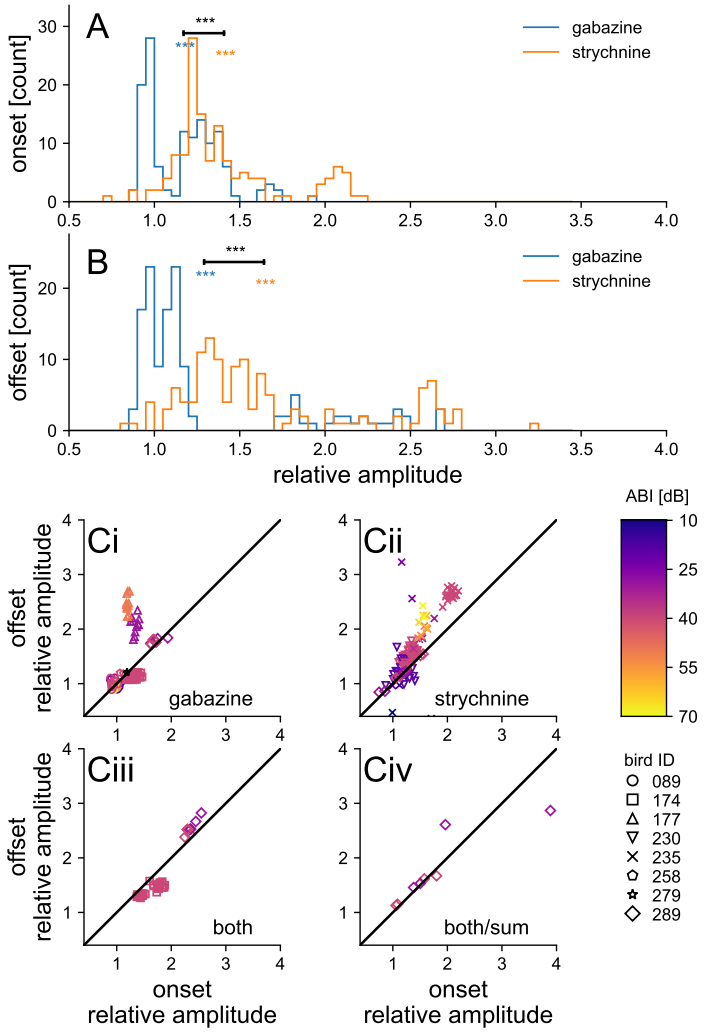

Figure 9: Population Responses to Pharmacology. Across the population, both gabazine and strychnine application significantly increased the onset and the offset responses with respect to the control condition. The response was measured as the average of first 50 ms of the low-pass filtered EFP after the stimulus onset/offset, and averaged across all ITDs.
A. Onset response, ratio to control condition. Gabazine: mean ± SE: 1.17 ± 0.02, $p = 3 \cdot 10^{-15}$, $N = 133$. Strychnine: 1.41 ± 0.03, $p = 6 \cdot 10^{-30}$, $N = 137$. The effect of strychnine was larger than that of gabazine ($p = 2 \cdot 10^{-11}$, Student's 2 population test). **B.** Offset response, ratio to control condition. Gabazine: 1.29 ± 0.05, $p = 3 \cdot 10^{-10}$, $N = 133$. Strychnine: 1.64 ± 0.05, $p = 4 \cdot 10^{-27}$, $N = 137$. Also for the offset, the effect of strychnine was larger than that of gabazine ($p = 9 \cdot 10^{-8}$). **Ci-Ciii.** Relative increase of the onset response (x-axis) and the offset response (y-axis) for different drug conditions and for the sum of gabazine and strychnine when measured independently in the same recording location. For both gabazine and strychnine, the increase of the offset was larger than that of the onset ($p = 0.0010$ and $p = 3 \cdot 10^{-5}$, respectively). Stimulus amplitude is shown with the color scale. The stimulus frequency, spanning from 3.2 kHz to 6.8 kHz, did not systematically affect the relative increase.
Civ. Non-linearity of GABA and glycine effects: for simultaneous administration of gabazine and strychnine ('both') the effect on both onset and offset was larger than expected from the 'sum' of both drugs administered independently (both/sum > 1) .

Discussion

GABAergic terminals surround all NL neurons (Carr et al., 1989). These inhibitory inputs should protect NL neurons from losing their ITD sensitivity when sound levels increase (Grün et al., 1991; Peña et al., 1996). To examine the role of inhibition in encoding ITD, we isolated inhibitory synaptic currents from extracellular field potentials in the NL of barn owls through the iontophoretic application of blockers of GABA or glycine. Both blockers caused significant increases in the low spectral frequencies of the field potential that are associated with synaptic potentials (Kuokkanen et al., 2018; McColgan et al., 2019), but did not affect the ITD tuning of responses in NL. Furthermore, synaptic activation profiles suggest that the inhibitory inputs to NL could originate from the primary-like and offset response types of the SON.

The Role of Inhibition in ITD coding

Inhibition in ITD coding has been the subject of extensive research (for reviews see Roberts et al., 2013; Yin et al., 2019). In small mammals, fast glycinergic inhibition contributes to the best ITD of responses in the medial superior olive (Franken et al., 2015; Leibold and Grothe, 2015) in a physiologically appropriate fashion. In birds, however, GABAergic inhibition in NL appears instead to increase the dynamic range of ITD sensitive responses in NL (Grün et al., 1991; Peña et al., 1996; Nishino et al., 2008) and not alter ITD tuning. *In vitro* studies further support a direct effect of inhibition on coincidence detection (Brückner and Hyson, 1998; Funabiki et al., 1998), where inhibition speeds the kinetics of excitatory postsynaptic potentials, thus reducing the duration of the coincidence window.

For our study, it is likely that the iontophoretic application of gabazine in NL blocked $GABA_A$ inhibition directly and locally, leading to the observed increases in activity (Fig. 9). It is also possible that the increased NL input to SON could also lead to SON inhibition of the NM inputs to NL, and thus decreased drive to NL. The local block probably dominates the indirect effects from the SON, although the different roles for inhibitory activity discussed below must be considered in a system with activity-dependent feedback.

In NL, $GABA_A$ signaling is depolarizing (Hyson et al., 1995). The GABAergic input activates

low threshold K+ conductances to decrease the membrane time constant and improve coincidence detection (Ashida et al., 2007; Kuba et al., 2003, 2005). Chicken NL also contains abundant $GABA_B$ receptors (Burger et al., 2005; Tang et al., 2009), shown to have a largely presynaptic action (Tang et al., 2009). Future studies might address the complex interactions among $GABA_B$ and metabotropic glutamate receptors *in vivo*.

The avian auditory brainstem nuclei exhibit a diversity of inhibitory transmission that suggests differential glycine, $GABA_A$ and $GABA_B$ receptor activity, tailored to roles in NM, NL, and NA (Lu et al., 2018). These distinct roles are supported by the presence of divergent inputs from the SON (Kuo et al., 2009; Baldassano and MacLeod, 2024; Burger et al., 2005). Furthermore, it seems likely that glycine may be co-released with GABA (Kuo et al., 2009; Coleman et al., 2011; Fischl et al., 2014). These *in vitro* results were supported by our iontophoresis of strychnine, which on its own typically did not affect the recorded potential in NL, but revealed a pronounced synergy when iontophoresed with gabazine (Fig. 9).

Results from our study support the observation that neither GABAergic nor glycinergic inhibition shifts ITD tuning. Instead, the effects of synaptic blockers support the observations of Peña et al. (1996) and are consistent with providing an increased dynamic range. We also observed varying profiles of synaptic activation, consistent with inputs from different SON cell types. Profiles of synaptic activation revealed more prominent inhibition following stimulus offset, suggesting inputs to NL might originate from both the primary-like and offset response types of the SON. These heterogeneous synaptic responses may represent separate SON neuronal populations and allow for additional regulation of ITD coding.

Frequency dependent changes in inhibition have been observed in chicken NL, potentially related to the coupling between their ears affecting low frequencies (Nishino et al., 2008). Nishino found that the level dependent suppression of firing rate at unfavorable ITDs was most prominent in low best frequency NL. In barn owls, however, loose patch recordings from NL neurons (Peña et al., 1996) revealed ITD sensitivity over the entire frequency range, and wide range of sound levels. We observed similar ITD sensitivity over the range of best frequencies and sound levels tested in this study, in contrast to the results in chickens (Nishino et al., 2008; Tang and Lu, 2012).

In vivo physiology in SON

The projections of the SON in the barn owl resemble those in chicken (Nishino et al., 2008; Von Bartheld et al., 1989; Coleman et al., 2011) and zebra finch (Wild et al., 2010). Similarly, most of the units we recorded in SON resembled those recorded in chicken (Tabor et al., 2012; Lachica et al., 1994). In both barn and chicken, SON recordings were largely binaural, and characterized by a majority of sustained response units, and a smaller number suppressed by sound. A previous study in barn owl (Moiseff and Konishi, 1983) had found both monaural and binaural responses, consistent with direct inputs from the ipsilateral NA and NL (Takahashi and Konishi, 1988). The heterogeneous response types may represent separate SON neuronal populations projecting to different nuclei (Burger et al., 2005; Baldassano and MacLeod, 2024).

Models of Inhibitory Synaptic Potentials

In our previous analysis of synaptic potentials in NL (McColgan et al., 2019), we isolated *in vivo* AMPA sensitive responses from the neurophonic in NL, using iontophoretic application of the antagonist NBQX. In low pass filtered responses, we subtracted the NBQX condition from the control condition to reveal synaptic contributions to the EFP. We found that the temporal dynamics of the evoked synaptic contributions were consistent with synaptic short-term depression (STD) (Tsodyks and Markram, 1997), and that the estimated time constants of an STD model fitted to the data were similar to the fast time constants reported from *in vitro* experiments in the chick (Kuba et al., 2002; Cook et al., 2003).

Our attempt to similarly model the time constants of GABAergic potentials in NL did not yield consistent results. We hypothesize that the large synaptic offset-effect stems from a combination of synaptic facilitation (Tsodyks and Markram, 1997) and possibly offset-type responses of SON neurons projected to NL, but testing the hypothesis either directly or by modeling was beyond the current study. There are significant reasons for our inability to fit time constants to these inhibitory potentials. The excitatory AMPA synapse in NL conveys first-order excitation from NM, with little modification, and may therefore be more constrained than the feedback from the SON, which involves monaural and binaural input, and multiple cell types. Thus, our models may have been under-constrained by the data, and did not permit us to explain the time course

of inhibitory potentials solely by models of synaptic depression and/or facilitation. Adding more variables to the model, however, would have led to over-fitting because of the nature of the time course measurements. The responses to both $GABA_A$ and glycine blockers were robust, but we conclude that future models would require incorporation of feedback loop kinetics, and multiple sources of inhibition such as the sustained and offset response types of SON.

Declaration of conflicting interest: No conflicts of interest, financial or otherwise, are declared by the authors.

Acknowledgments: We thank Go Ashida for helpful discussions, Sarada Viswanathan for her help with the viral tracers and Waisudin Kamal for his assistance with cell counts.

Funding statement: Supported by NSF CRCNS IOS1516357, by the National Institute on Deafness and Other Communications Disorders (NIDCD DC00436 and DC019341), and the Bundesministerium für Bildung und Forschung (BMBF): German – US-American collaboration "Field Potentials in the Auditory System" as part of the NSF/NIH/ANR/BMBF/BSF CRCNS program, 01GQ1505A and 01GQ1505B. The research was further funded by the Deutsche Forschungsgemeinschaft (DFG, German Research Foundation) grant nr. 502188599.

Ethical approval and informed consent statement: All animal care and experimental procedures were conducted following NIH guidelines and approved by the University of Maryland Institutional Animal Care and Use Committee. Efforts were made to minimize animal suffering and reduce the number of animals used.

References

Abdi H, Bonferroni and šidák corrections for multiple comparisons In: Encyclopedia of measurement and statistics, edited by Salkin N. Sage, Thousand Oaks, CA, US, 2007 p. 103 – 107.

Agmon-Snir H, Carr CE, Rinzel J. The role of dendrites in auditory coincidence detection. Nature 393: 268–272, 1998.

Ashida G, Abe K, Funabiki K, Konishi M. Passive soma facilitates submillisecond coincidence detection in the owl's auditory system. J. Neurophysiol. 97: 2267–2282, 2007.

Baldassano JF, MacLeod KM. Electrophysiological correlates of divergent projections in the avian superior olivary nucleus. J. Neurophysiol. 132: 1412–1425, 2024.

Brückner S, Hyson RL. Effect of GABA on the processing of interaural time differences in nucleus laminaris neurons in the chick. Eur. J. Neurosci. 10: 3438–3450, 1998.

Burger RM, Forsythe ID, Kopp-Scheinpflug C. Editorial: Inhibitory function in auditory processing. Front Neural Circuits 9, 2015.

Burger RM, Cramer KS, Pfeiffer JD, Rubel EW. Avian superior olivary nucleus provides divergent inhibitory input to parallel auditory pathways. J. Comp. Neurol. 481: 6–18, 2005.

Burger RM, Fukui I, Ohmori H, Rubel EW. Inhibition in the balance: binaurally coupled inhibitory feedback in sound localization circuitry. J. Neurophysiol. 106: 4–14, 2011.

Burger RM, Pfeiffer JD, Westrum LE, Bernard A, Rubel EW. Expression of GABA(B) receptor in the avian auditory brainstem: ontogeny, afferent deprivation, and ultrastructure. J. Comp. Neurol. 489: 11–22, 2005.

Burger R, Rubel E, Encoding of interaural timing for binaural hearing In: The senses: a comprehensive reference, edited by Dallos P, Oertel D, Vol. 3. Elsevier, 2008 p. 613–630.

Carr CE, Fujita I, Konishi M. Distribution of GABAergic neurons and terminals in the auditory system of the barn owl. J. Comp. Neurol. 286: 190–207, 1989.

Code RA, Burd GD, Rubel EW. Development of GABA immunoreactivity in brainstem auditory nuclei of the chick: Ontogeny of gradients in terminal staining. J Comp Neurol 284: 504–518, 1989.

Coleman WL, Fischl MJ, Weimann SR, Burger RM. GABAergic and glycinergic inhibition modulate monaural auditory response properties in the avian superior olivary nucleus. J. Neurophysiol. 105: 2405–2420, 2011.

Conlee JW, Parks TN. Origin of ascending auditory projections to the nucleus mesencephalicus lateralis pars dorsalis in the chicken. Brain Res 367: 96–113, 1986.

Cook DL, Schwindt PC, Grande LA, Spain WJ. Synaptic depression in the localization of sound. Nature 421: 66–70, 2003.

Dasika VK, White JA, Carney LH, Colburn HS. Effects of inhibitory feedback in a network model of avian brain stem. J. Neurophysiol. 94: 400–414, 2005.

Fischl MJ, Burger RM. Glycinergic transmission modulates GABAergic inhibition in the avian auditory pathway. Front Neural Circuit 8: 19, 2014.

Fischl MJ, Weimann SR, Kearse MG, Burger RM. Slowly emerging glycinergic transmission enhances inhibition in the sound localization pathway of the avian auditory system. J. Neurophysiol. 111: 565–572, 2014.

Franken TP, Roberts MT, Wei L, Golding NL, Joris PX. In vivo coincidence detection in mammalian sound localization generates phase delays. Nat Neurosci 18: 444–452, 2015.

Fukui I, Burger RM, Ohmori H, Rubel EW. GABAergic inhibition sharpens the frequency tuning and enhances phase locking in chicken nucleus magnocellularis neurons. J. Neurosci. 30: 12075–12083, 2010.

Funabiki K, Koyano K, Ohmori H. The role of GABAergic inputs for coincidence detection in the neurones of nucleus laminaris of the chick. J. Physiol. 508: 851–869, 1998.

Grün S, Wagner H, Carr C, Aertsen A 1991 Binaural Interaction in the Nucleus Laminaris of the Barn Owl : A Quantitative Model Research Report BrainWorks 1991-01, MPI for Biological Cybernetics.

Hyson RL, Reyes AD, Rubel EW. A depolarizing inhibitory response to GABA in brainstem auditory neurons of the chick. Brain Res 677: 117–126, 1995.

Köppl C, Carr CE. Computational diversity in the cochlear nucleus angularis of the barn owl. J. Neurophysiol. 89: 2313–2329, 2003.

Kraemer A, Carr CE 2017 Response types of the superior olivary nucleus of the barn owl In: Society for Neuroscience, p. 585.11.

Kuba H, Koyano K, Ohmori H. Synaptic depression improves coincidence detection in the nucleus laminaris in brainstem slices of the chick embryo. Eur J Neurosci 15: 984–990, 2002.

Kuba H, Yamada R, Fukui I, Ohmori H. Tonotopic specialization of auditory coincidence detection in nucleus laminaris of the chick. J. Neurosci. 25: 1924–1934, 2005.

Kuba H, Yamada R, Ohmori H. Evaluation of the limiting acuity of coincidence detection in nucleus laminaris of the chicken. J. Physiol. 552: 611–620, 2003.

Kuo SP, Bradley LA, Trussell LO. Heterogeneous kinetics and pharmacology of synaptic inhibition in the chick auditory brainstem. J. Neurosci. 29: 9625–9634, 2009.

Kuokkanen PT, Ashida G, Carr CE, Wagner H, Kempter R. Linear summation in the barn owl's brainstem underlies responses to interaural time differences. J. Neurophysiol. 110: 117–130, 2013.

Kuokkanen PT, Ashida G, Kraemer A, McColgan T, Funabiki K, Wagner H, Köppl C, Carr CE, Kempter R. Contribution of action potentials to the extracellular field potential in the nucleus laminaris of barn owl. J. Neurophysiol. 119: 1422–1436, 2018.

Kuokkanen PT, Wagner H, Ashida G, Carr CE, Kempter R. On the origin of the extracellular field potential in the nucleus laminaris of the barn owl. J. Neurophysiol. 104: 2274–2290, 2010.

Lachica EA, Rübsamen R, Rubel EW. GABAergic terminals in nucleus magnocellularis and laminaris originate from the superior olivary nucleus. J. Comp. Neurol. 348: 403–418, 1994.

Leibold C, Grothe B. Sound localization with microsecond precision in mammals: What is it we do not understand? e-Neuroforum 6: 3–10, 2015.

Lu Y, Liu Y, Curry RJ. Activity-dependent synaptic integration and modulation of bilateral excitatory inputs in an auditory coincidence detection circuit. The J Physiol 596: 1981–1997, 2018.

MacLeod KM. Short-term synaptic plasticity and intensity coding. Hear Res 279: 13–21, 2011.

MacLeod KM, Pandya S. Expression and neurotransmitter association of the synaptic calcium sensor synaptotagmin in the avian auditory brain stem. J Assoc for Res Otolaryngol 23: 701–720, 2022.

McColgan T, Kuokkanen PT, Carr CE, Kempter R. Dynamics of synaptic extracellular field potentials in the nucleus laminaris of the barn owl. J. Neurophysiol. 121: 1034–1047, 2019.

Moiseff A, Konishi M. Binaural characteristics of units in the owl's brainstem auditory pathway: precursors of restricted spatial receptive fields. J. Neurosci. 3: 2553–2562, 1983.

Monsivais P, Rubel EW. Accommodation Enhances Depolarizing Inhibition in Central Neurons. J. Neurosci. 21: 7823–7830, 2001.

Monsivais P, Yang L, Rubel EW. GABAergic inhibition in nucleus magnocellularis: implications for phase locking in the avian auditory brainstem. J. Neurosci. 20: 2954–2963, 2000.

Nishino E, Ohmori H. The Modulation by Intensity of the Processing of Interaural Timing Cues for Localizing Sounds. Mol Neurobiol 40: 157–165, 2009.

Nishino E, Yamada R, Kuba H, Hioki H, Furuta T, Kaneko T, Ohmori H. Sound-intensity-dependent compensation for the small interaural time difference cue for sound source localization. J. Neurosci. 28: 7153–7164, 2008.

Peña JL, Viete S, Albeck Y, Konishi M. Tolerance to sound intensity of binaural coincidence detection in the nucleus laminaris of the owl. J. Neurosci. 16: 7046–7054, 1996.

Quian Quiroga R, Nadasdy Z, Ben-Shaul Y. Unsupervised spike detection and sorting with wavelets and superparamagnetic clustering. Neural computation 16: 1661–1687, 2004.

Reyes AD, Rubel EW, Spain WJ. In vitro analysis of optimal stimuli for phase-locking and time-delayed modulation of firing in avian nucleus laminaris neurons. J. Neurosci. 16: 993–1007, 1996.

Roberts MT, Seeman SC, Golding NL. A Mechanistic Understanding of the Role of Feedforward Inhibition in the Mammalian Sound Localization Circuitry. Neuron 78: 923–935, 2013.

Tabor KM, Coleman WL, Rubel EW, Burger RM. Tonotopic organization of the superior olivary nucleus in the chicken auditory brainstem. J Comp Neurol 520: 1493–1508, 2012.

Takahashi TT, Konishi M. Projections of nucleus angularis and nucleus laminaris to the lateral lemniscal nuclear complex of the barn owl. J Comp Neurol 274: 212–238, 1988.

Takahashi Y, Konishi M. Manipulation of inhibition in the owl's nucleus laminaris and its effects on optic tectum neurons. Neuroscience 111: 373–378, 2002.

Tang ZQ, Gao H, Lu Y. Control of a Depolarizing GABAergic Input in an Auditory Coincidence Detection Circuit. J. Neurophysiol. 102: 1672–1683, 2009.

Tang ZQ, Lu Y. Two GABAA responses with distinct kinetics in a sound localization circuit. The J Physiol 590: 3787–3805, 2012.

Tervo DGR, Hwang BY, Viswanathan S, Gaj T, Lavzin M, Ritola KD, Lindo S, Michael S, Kuleshova E, Ojala D, Huang CC, Gerfen CR, Schiller J, Dudman JT, Hantman AW, Looger LL, Schaffer DV, Karpova AY. A Designer AAV Variant Permits Efficient Retrograde Access to Projection Neurons. Neuron 92: 372–382, 2016.

Tsodyks M, Markram H. The neural code between neocortical pyramidal neurons depends on neurotransmitter release probability. Proc. Natl. Acad. Sci. USA 94: 719–723, 1997.

Von Bartheld CS, Code RA, Rubel EW. GABAergic neurons in brainstem auditory nuclei of the chick: Distribution, morphology, and connectivity. J Comp Neurol 287: 470–483, 1989.

Wild JM, Krützfeldt NO, Kubke MF. Connections of the auditory brainstem in a songbird, Taeniopygia guttata . III. Projections of the superior olive and lateral lemniscal nuclei. J Comp Neurol 518: 2149–2167, 2010.

Winer JA, Larue DT, Pollak GD. GABA and glycine in the central auditory system of the mustache bat: Structural substrates for inhibitory neuronal organization. J Comp Neurol 355: 317–353, 1995.

Yang L, Monsivais P, Rubel EW. The superior olivary nucleus and its influence on nucleus laminaris: a source of inhibitory feedback for coincidence detection in the avian auditory brainstem. J. Neurosci. 19: 2313–2325, 1999.

Yin TC, Smith PH, Joris PX. Neural mechanisms of binaural processing in the auditory brainstem. Compr Physiol 9: 1503–1575, 2019.